International Journal of Greenhouse Gas Control 87 (2019) 121–133

Contents lists available at ScienceDirect

International Journal of Greenhouse Gas Control

journal homepage: www.elsevier.com/locate/ijggc

Gas flow through shallow sediments—A case study using passive and active seismic field data

Martin Landrø[a,*], Daniel Wehner[b], Noralf Vedvik[b], Philip Ringrose[b], Nora Løw Løhre[b], Karl Berteussen[c]

[a] Department of Electronic Systems, NTNU, Trondheim, Norway
[b] Department of Geoscience and Petroleum, NTNU, Trondheim, Norway
[c] GFF as, Oslo, Norway

ARTICLE INFO

Keywords:
CO_2 storage
Time-lapse seismic
Gas flow in shallow sediments
CO_2 leakage
Gas leakage
Geophysics

ABSTRACT

Offshore Quaternary sediment sequences are generally weak and unconsolidated, and fluid flow through these rock formations is hard to predict or model. Surface flow observations, such as gas seeps, often appear random and may be controlled by the architecture and facies distribution within the shallow strata. Using geophysical data acquired before and after a sub-seabed blowout from a 4700m-deep interval in a North Sea hydrocarbon exploration well, we investigate the nature of subsurface gas flow behaviour in shallow sediment sequences. The underground gas blow-out lasted for a period of almost one year, and when the flow from the deep gas reservoir was stopped, we observed that fluids continued to flow in the shallow subsurface and probably continue to this day, almost 30 years later.

During the underground blowout phase, passive seismic data revealed episodes of up to 30 min with high seismicity followed by quieter periods of several hours. Time-lapse seismic data revealed that gas had migrated into several shallow sand layers, and that this migration had continued over for at least 25 years. The seismic data also indicated that gas entered into a shallow tunnel valley complex approximately 1–2 years after the blowout, and at a later stage migrated further. The 3D seismic data also shows indications of gas leakage outside the well bore of the relief well, drilled through the overburden sediments 1.2 km away from the main well. This implies that wells drilled through weak overburden rocks can weaken the formations potentially creating vertical pathways for gas migration. The observations from this gas migration case history are used to gain more general insights into the flow of buoyant gases, especially CO_2, in shallow unconsolidated sediment sequences.

1. Introduction

A key issue in geological storage of CO_2 is to minimize the risk of leakage through overburden rock layers. If CCS (Carbon Capture and Storage) becomes a common tool to reduce CO_2 emissions to the atmosphere in the future, it will be essential to have detailed knowledge about how leakage events might develop and especially to study possible migration paths through the overburden. For many regions, the most likely sites for CO_2 storage are to be found offshore, partly due to large accessible storage volumes and partly due to easier public acceptance. In this respect, it is useful to use natural gas as a proxy for the migration of CO_2 and to study hydrocarbon gas flow through shallow overburden. The phase behaviour of CO_2 is highly dependent on depth and temperature, normally being in the liquid or dense phase in the storage unit but entering into the gas phase in shallower units in the case of vertical migration or leakage. Due to the lack of availability of useful gas-phase CO_2 migration case studies we use methane as a proxy for understanding possible CO_2 migration processes. The validity and relevance of using methane gas as a proxy to CO_2 has been discussed by several scientists (e.g. Benson and Hepple, 2005; Grimstad et al., 2009). Fig. 1 shows typical fluid density functions for CO_2 and CH_4 in the top 1000 m sediment column in an offshore North Sea basin setting, using calibration data from the Sleipner CO_2 storage site (Nooner et al., 2007; Singh et al., 2010; Landrø and Zumberge, 2017). At the depths discussed in this paper, gas-phase CO_2 will be approximately 3 to 4 times denser than CH_4 (shallower than 500 m), but then 10 to 14 times denser below 500 m as CO_2 enters the liquid and dense phases. Both CO_2 and CH_4 are dominantly non-wetting phases and are trapped in water-filled sediments by capillary interfaces. Since the interfacial tension for CO_2-brine systems is generally lower than for CH_4-brine systems (Naylor

* Corresponding author.
E-mail address: Martin.Landro@ntnu.no (M. Landrø).

https://doi.org/10.1016/j.ijggc.2019.05.001
Received 18 September 2018; Received in revised form 29 April 2019; Accepted 1 May 2019

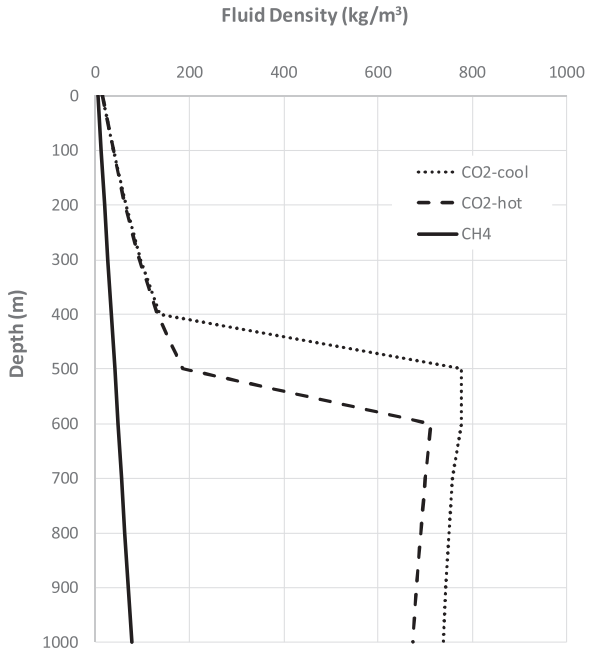

Fig. 1. Density profiles for CH_4 and CO_2 for typical conditions in the top 1000 m sediment column in an offshore North Sea basin setting. Geothermal gradient is assumed to be between 35degC/km or 30degC/km (CO_2-cool case) to illustrated the range of CO_2 properties. Seabed temperature is set to 5degC and brine density set to 1020 kg/m3, using typical values from Nooner et al. (2007) and Singh et al. (2010).

et al., 2011), the buoyancy force for CO_2 will be slightly higher than the density ratio. For example, at 500 m depth gas-phase CO_2 will be around 2.5 less buoyant than CH_4. CO_2 is also around 100 times more soluble in water than CH_4, so migrating CO_2 will experience more losses due to dissolution during migration, as observed in shallow CO_2 migration experiments (Cevatoglu et al., 2015). Accepting these differences, we argue that migration of CH_4 in shallow sediments is a reasonable analogue for CO_2 migration.

2. Background

2.1. The 1989 underground blow out

In January 1989 a deep exploration well (2/4-14) drilled by Saga Petroleum came out of control due to extremely high reservoir pressures (above 1000 bar) that occurred at a depth of 4.7 km. This well is located at 56° 41′ 5.26″ N and 3° 8′ 43.08″ E in the southern part of the Norwegian North Sea (Fig. 2). The blow out preventer was activated and ensured no leakage of hydrocarbons into the water column. However, the well leaked through a gap in the steel casing at approximately 1360 m depth, and the gas flow entered the region outside the outer casing at a depth of approximately 900 m. Hence, the event developed into a subsurface blow out. The blow out lasted for almost a year, and the underground flow was eventually killed by pumping heavy mud into the reservoir from a relief well (2/4-15) that was drilled close to the 2/4-14 well.

In this paper we will use this event and various seismic data sets that were acquired by Saga during the active period of un-controlled subsurface flow to study how gas migrates through a heterogeneous sedimentary overburden. We will focus on both vertical and horizontal migration of gas, and we make an attempt to describe the extent and movement of the gas flow as a function of calendar time. The objective of this paper is to use this case study as a proxy to study CO_2-leakage from a potential storage site in a similar lithology (mixed sands and shales).

In order to understand the flow processes through shallow sand layers below the seabed, we designed a laboratory tank experiment where we injected air at the base to study variability in the flow patterns. A video sequence recorded at the seabed close to well 2/4-14 eleven months after the blowout is used for comparison with the tank experiment. In addition, we use seismic data acquired in 1988 (pre-blowout), 1990 (1.5 years after the blowout) and 2009 (20 years after the blowout) to map the long term migration of gas through the shallow sedimentary layers and into the water column.

Zadeh and Landrø (2011) used time-lapse seismic refraction data to map shallow gas accumulations close to the blow out well. They estimated that the shallowest gas-filled layer was situated approximately 170 m below the sea surface. Haavik and Landrø (2014) found that natural shallow gas accumulations were also present in the area close to the 2/4-14 well (the blowout well) demonstrating the importance of differentiating man-induced gas leakage from gases that have migrated over geological time periods. Natural seepage of hydrocarbon gases (mainly methane) from the subsurface to the surface is widely observed and discussed by for instance by Etiope (2015); Haavik and Landrø (2014) and Hovland and Judd (1988). Methane is also widespread in sedimentary rock systems, being generated by thermogenic processes in deeper petroleum systems and by biogenic processes in shallower rock units. In the following analysis, we assume the observed gases are methane (based on available well data), but minor components of heavier hydrocarbons and CO_2 could be present in these gases. Blackford et al. (2014) presented a controlled CO_2 leakage study in which CO_2 was injected 11 m below seabed and monitored by seismic reflection profiles and multibeam sonar data. Their time-lapse seismic data shows a clear bright spot beneath a fine sand layer at day 13, approximately 2–3 m below the seabed. Three weeks later, the seismic data showed a chimney extending to the seafloor, and multibeam data was used to confirm that gas has escaped into the water layer.

3. Database and methods

3.1. Seismic data

This work is based on 2D site survey seismic data acquired using a 1 km long hydrophone streamer. The data was acquired in 1988 (prior to the blow-out), and repeated again in 1990 and 2009. We refer to Larsen and Lie (1990) and Landrø (2011) for a comprehensive overview of various vintages of seismic datasets that were recorded. A 3D seismic dataset was acquired in 1991, and Fig. 3 shows an in-line section from this data set. Two vertical chimneys close to the two wells (the blow out well and the relief well) are observed, as well as a bright spot that is interpreted as the top of a gas-charged sand layer at 490 m depth. An example of time lapse seismic data using the single 2D line is shown in Fig. 4, where we can observe clear differences for the same sand layer between the three seismic vintages. In 1988 (prior to the sub-seabed blow out) the top of the thin sand layer (shown by a black arrow) at approximately 520 ms shows a moderate amplitude that is significantly increased in 1990 and 2009. This brightening is interpreted as being caused by gas flowing horizontally in this thin layer. A significant pulldown for this event, close to the well is clearly visible in Fig. 4. This is likely caused by the presence of gas above this thin layer at 490 m, indicating that some gas had migrated above 490 m by 1990. This pull down is less pronounced in 2009, indicating that the amount of gas above the sand layer at the well position has decreased between 1990 and 2009.

A RMS amplitude map of the interpreted top reflection of this sand layer is shown in Fig. 5, where we observe a close-to-circular shaped anomaly centred around the 14-well. The dashed blue line in Fig. 5 shows the extent of the gas anomaly estimated by Saga in September 1989, approximately 9 months after the blow out. We observe that the average radius of the gas anomaly has increased from 0.8 km in September 1989 to 1.2 km in 1991. In the period from 23rd September

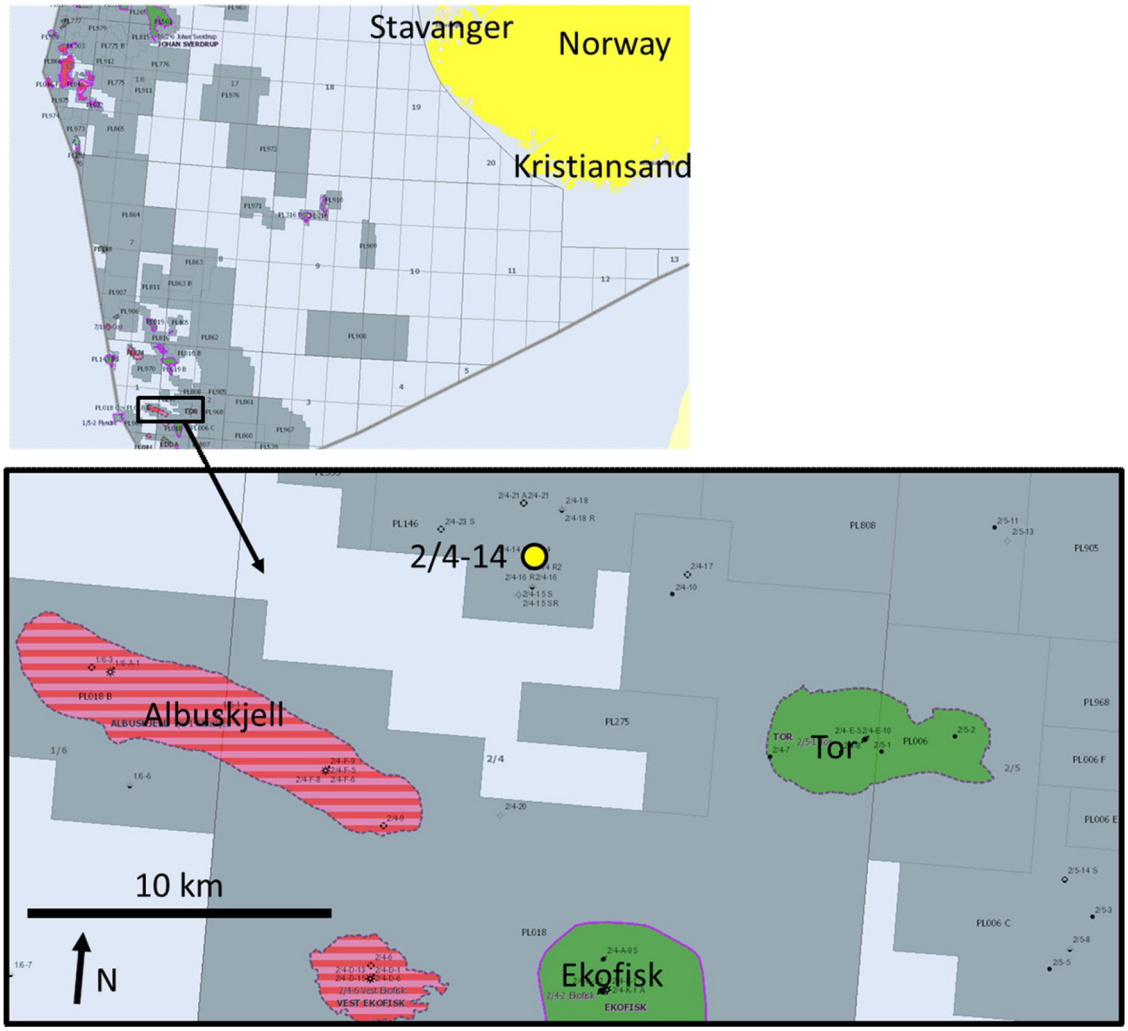

Fig. 2. Location map of the 2/4-14 well. The well is situated in the southern part of the Norwegian part of the North Sea, approximately 20 km North of the Ekofisk field, close to the UK (to the West) and Danish (to the South) borders.

1989 to 3rd October 1989, Read Well Services installed four geophones at the seabed, close to the 2/4-14 well, recording the noise bursts from the underground flow that was still active at that time. This shows that at the time of the passive seismic data acquisition, the extent of the gas anomaly in the 490 m sand layer was approximately 0.8 km. Although these data have not been made directly available to us in digital format in this project, we are able to present some of the results from this passive seismic study here.

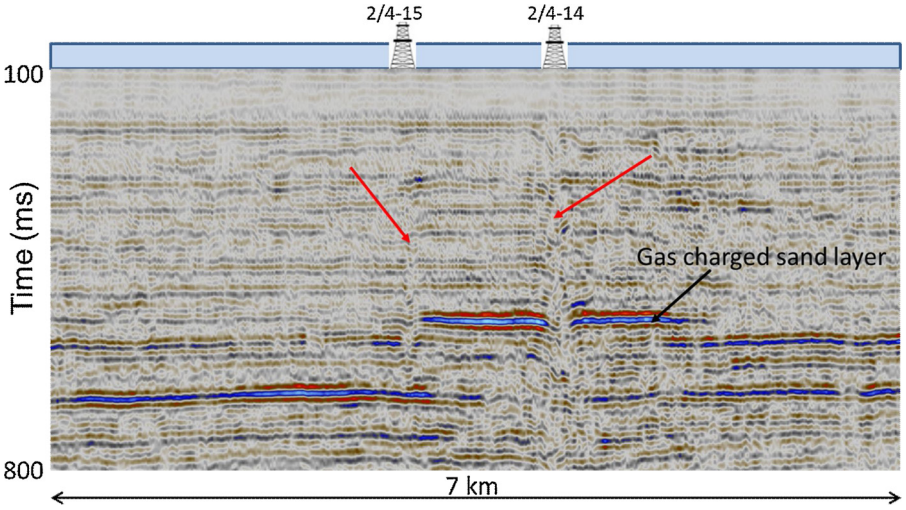

Fig. 3. Vertical profile (Line A shown in Fig. 4) from the 1991 3D seismic data. The blowout well is 2/4-14, and the relief well is 2/4-15 that was drilled in 1989. The red arrows show interpreted vertical gas chimneys close to the well path. The bright seismic event is a gas charged thin sand layer, where the gas extends approximately 1 km to each side of the 2/4-14 well.

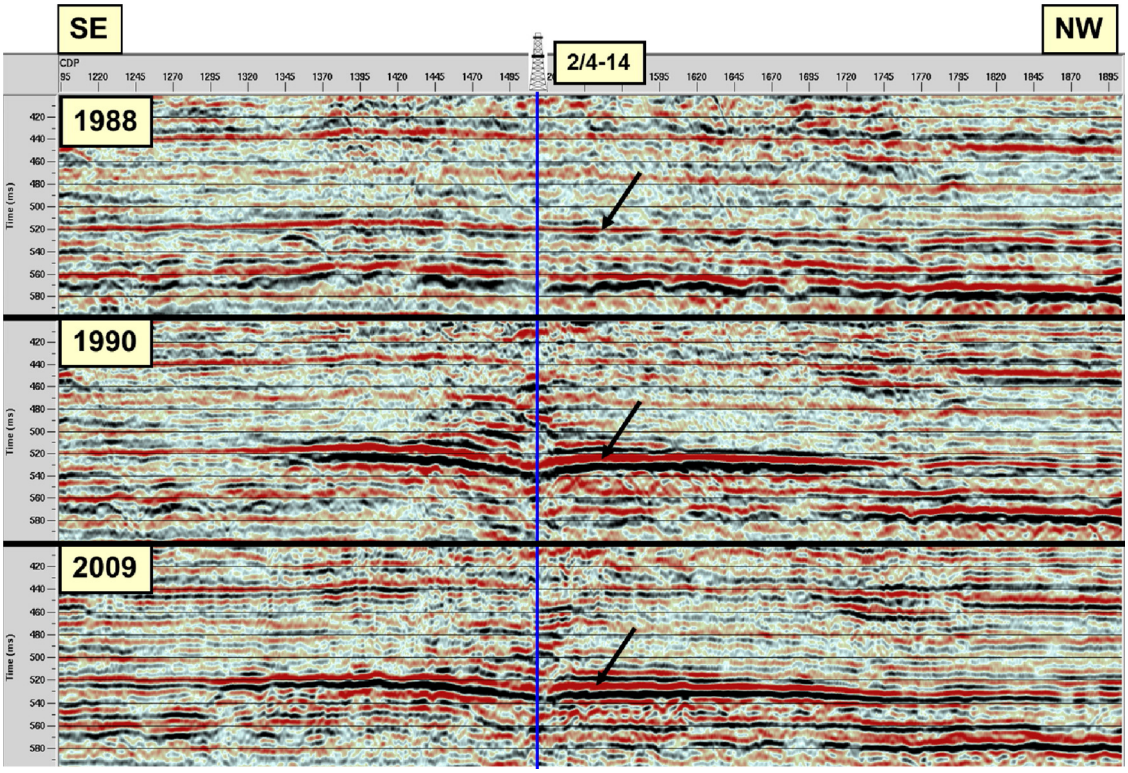

Fig. 4. Time lapse seismic data acquired prior to the underground blow out (1988), one year after the blow out (1990) and 20 years after (2009) for line B (see Fig. 5). Notice the brightening of the reflection at approximately 520 ms. This event represents the top of a thin sand layer at approximately 490 m depth. Notice that the pull down close to the well is less pronounced in 2009 compared to 1990, indicating less amount of gas directly above this layer close to the well. Also note that the extent of the gas anomaly has increased somewhat between 1990 and 2009. The figure is modified from Landrø (2011). The length of this section is 4.4 km, and the two-way traveltime for each of three sections are from 400 to 600 ms.

3.2. Other data and observations

In addition to seismic data we have access to video recordings showing gas bubbles emerging at the seabed close to the 2/4-14 well. Furthermore, we designed a simple laboratory flow experiment using fine-grained sand in a water tank, with air injected at the base of the tank, in order to replicate gas migration processes in unconsolidated sediments.

3.3. Time lapse seismic analysis

Larsen and Lie (1990) were among the first to present time-lapse seismic analysis from the 2/4-14 underground blow out. The target depth for this study was shallow, approximately 500 m, and the formation lithology was mainly sandstone. There are two complementary ways of analysing time-lapse seismic data: first to look for amplitude differences and map those over the study area and second to estimate travel time shifts (Landrø et al., 1999; Calvert, 2005; Landrø, 2015). In the present work we will use travel time shifts between various vintages as the main tool, but we will also map and show the amplitude anomalies that occur associated with shallow sand layers that have been charged with gas. The traveltime differences between the 1988 and 2009 site survey data for the seabed reflection are minimal, less than 0.5 ms on average. To further minimize the error caused by slight differences in source and receiver positions, we aligned the seabed reflection arrival times between two surveys prior to the time shift analysis.

3.4. Tunnel valleys

Tunnel valleys are observed in the first few hundred metres of sediment cover over most of the North Sea basin (van der Vegt et al., 2012). The tunnel valleys are sub-glacial channel features created beneath, or in front of, ice sheets from the Pleistocene glaciations. Tunnel valley widths are between 1 and 10 km and they can penetrate down to a couple of hundred meters (Stewart et al., 2013; Furre et al., 2014). The tunnel valley systems are typically buried by a thin cover of Holocene sediments.

At this site several tunnel valleys are observed approximately 30–40 m below the seabed, as shown in Fig. 6. Well 2/4-14 is drilled through one of these tunnel valleys. The type of sediment fill within the tunnel valleys is unknown, however, it is reasonable to assume that much of the fill is coarse-grained sand and gravel with higher porosity than the surrounding sediments (typically glacial outwash dominated by silts and clays). This interpretation is supported by the seismic time-lapse observations whereby the glacial channels represent high permeable units for gas flow. The thickness of the tunnel valley close to the 14-well is approximately 18 m.

4. Results and interpretation

4.1. Time lapse seismic analysis (200–750 m deep sand layers)

Fig. 7 shows an example of a 4D seismic difference between 2009 and 1990, a time span of 19 years for line B (same line as displayed in Fig. 4). We observe strong 4D anomalies for two-way traveltimes between 0.5 and 0.75 s (corresponding to a depth range of 470 to 750 m below sea surface). These anomalies are interpreted as saturation changes within thin sand layers. As shown by Landrø (2011), 4D time shift analyses reveal that these anomalies can be interpreted by a saturation pattern with less gas close to the well and more gas further away from the well. This observation is also in accordance with fluid flow simulations (Langseth and Landrø, 2012).

The shallow anomalies, observed between 0.25 to 0.4 s, very close

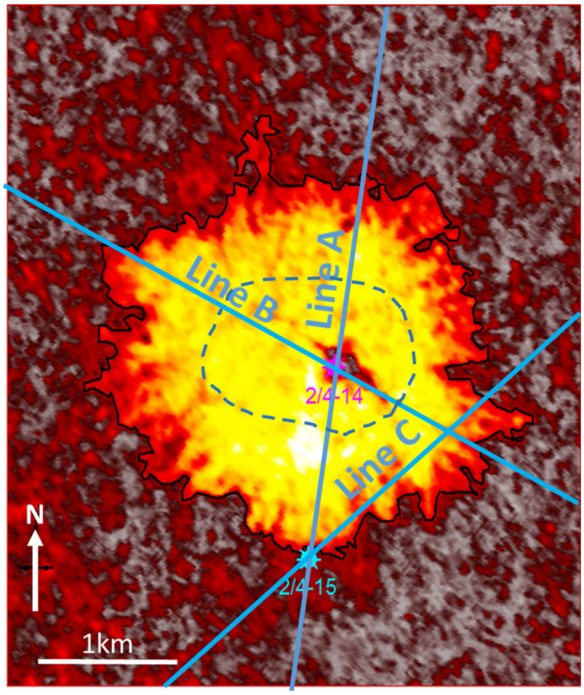

Fig. 5. Amplitude map (24 ms RMS window at top of the sand layer at 490 m depth). Notice the circular shape of the anomaly and that the anomaly extends to the relief well (2/4-15) to the south of the 2/4-14 well. Line A is extracted from the 3D seismic data acquired in 1991 (the same data set as is used to produce this amplitude map). Lines B and C are site survey data acquired prior to (1988) and after the underground blowout (1990). Lines B and C were also repeated in 2009. The blue dashed line shows the extent of the gas plume in September 1989 as interpreted from 2D site survey seismic data.

to the well are most likely caused by a slight increase in gas saturation in this region. This is confirmed by the negative time shift observed by Landrø (2011). However, there are only minor 4D differences in the very shallow regions in Fig. 7 (between 0.1 and 0.2 s). Does this indicate that there has been no migration of gas from the deeper sediments into the water layer? Probably not, since flow of gas through this layer might be small in volume and of a random nature, and might therefore be harder to detect.

4.2. Time shift analysis of shallow subsurface (< 100 m)

In the following section we focus on gas migration through the shallow section 100 m below the seabed. There are no well logs available covering this column. However, from XRD-analysis of drill cutting samples we find that the volumetric clay content is less than 10%, and the volumetric quartz content is close to 50%. This implies a porosity or around 40–50% in these shallow sediments (0–100 m below seabed), although there is considerable uncertainty in this estimate (see for instance Salem, 2000). The gamma log from deeper sections of the well (200–800 m) shows alternating sand and shale layers (Fig. 7 in Landrø, 2011). Some of these shale layers are thin, probably of the order of meters or less. It is therefore reasonable to assume (based on the XRD-analysis and the gammalog for deeper parts of the well) that the interval from the seabed and 100 m deeper is predominantly high porosity sand interbedded with some thin shale layers.

Fig. 8a shows a detailed time shift analysis for an interface situated approximately 95 m below the seabed. Here we use the simplest method for time shift estimation: picking the travel time of the maximum (or minimum) peak. Around the area of the tunnel valley (marked with a red double arrow on the figure) we observe time shifts of the order of 3–4 ms between 1988 and 1990. This is interpreted as gas migrating into sand layers above this level. Outside the tunnel valley area there is also a timeshift between 1988 and 1990, but much less, of the order of 1–2 ms and approaching zero approximately 1.2 km to the South East of the well and 1 km to the North West. In the 2009 data we notice that the timeshifts are reduced and that the situation within the tunnel valley area is nearly back to the pre-blowout situation. For the area outside the tunnel valley, there is hardly any change from 1990 to 2009. The most likely interpretation therefore, based on these traveltime shifts, is that the gas that leaked into the tunnel valley, has later migrated upwards into the water layer. For the area outside the tunnel valley, the most likely interpretation is to assume that there are only minor changes in gas saturation in the shallow sediments between 1990 and 2009.

Fig. 8b shows the results of a time-lapse refraction study along the same line. In a refraction study, we are not using the reflection signals as shown in Fig. 8a, but the far offset seismic data. In this way, time-lapse refraction analysis and time-lapse reflection analysis are complementary and independent of each other. From Fig. 8b we clearly observe a strong increase in time shifts between 1988 and 1990, up to 3 ms close to the well and the tunnel valley. A similar, but opposite time shift is observed from 1990 to 2009, indicating that the gas that was stored in the tunnel valley in 1990 has migrated away in 2009. Similar, but weaker anomalies are observed close to the second tunnel valley (in

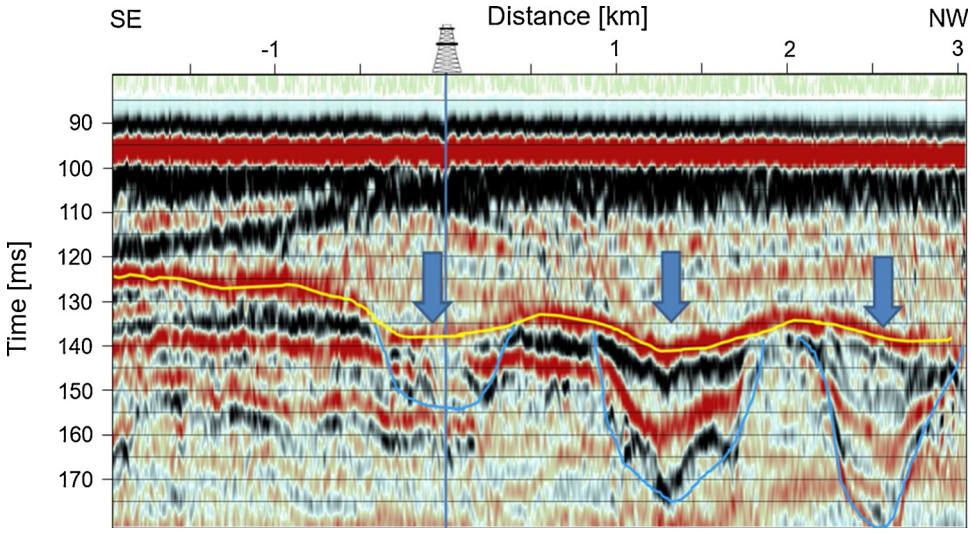

Fig. 6. Interpreted shallow tunnel valleys (shown by the three arrows) from the site survey data acquired in 1988 (Line B). The 2/4-14 well is drilled through one of the tunnel valleys. The depth of this tunnel valley is roughly 18 m (assuming a P-wave velocity of 1800 m/s for the shallow sediments), and the width is approximately 800 m. The distances to the two tunnel valleys in the Northwestern direction is 1.3 and 2.5 km, respectively.

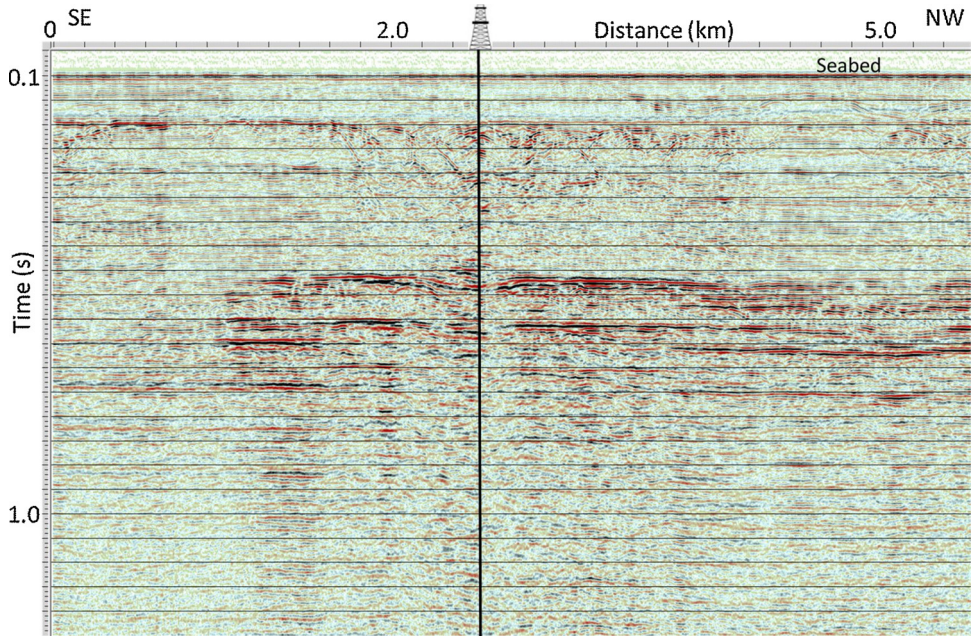

Fig. 7. 4D seismic difference between 2009 and 1990 (line B). Notice significant changes in the time interval between 0.5–0.8 s. Also notice some scattered anomalies close to the well for the shallow regions (between 0.2 and 0.5 s).

the North-western direction in Fig. 8b), and practically no time shifts are observed close to the third tunnel value (farthest away from the well position). This means that both time lapse reflection and refraction studies indicate the same trend: The tunnel valley that is penetrated by the 2/4-14 well has been gas charged and then the gas charge has been reduced as time has passed.

4.3. 3D seismic data

It is hard to estimate precisely the actual extent of the two vertical chimnies in Fig. 3, since the actual cross section is probably less than the seismic wavelength. Moser et al. (2016) discuss various methods to detect such vertical cylinder-shaped anomalies in seismic datasets using diffractions. Arntsen et al. (2007) present and discuss various aspects related to seismic modeling of such gas chimneys. Fig. 3 clearly shows the gas-charged sand layer at approximately 490 m depth. The gap in the middle of this bright seismic event is caused by presence of gas that has migrated outside the well bore above this sand layer. The presence of gas close to the well makes it hard to image the top of this sand layer since the gas acts as a shield that prevents seismic imaging along the vertical gas chimney. This explains why the two gas chimneys (marked by red arrows) appear as white or dim zones on the 3D seismic image. Fig. 9 illustrates the time lapse effect of the chimney close to the 15-well in more detail: by comparing estimated time lapse seismic time shifts between 1990 and 2009, we find that there is a significant increase in time shift close to the 15-well. This is probably caused by gas migrating along the vertical well path close to the 15-well in the period between 1990 and 2009.

4.4. The sand tank experiment

In order to obtain a qualitative understanding of gas flow through the uppermost 10 m below seabed, a dedicated sand tank experiment was conducted. Clean sand was put in a cylinder and filled with water, and air was injected at the bottom. As the air was released, a steady flow through the sand was established. Then, after 40–50 s, the air flow into the water stopped, and a fracture developed in the sand layer. As this fracture closed an air bubble escaped into the water, followed by a steady flow of air bubbles again at a new location. The air flow rate was constant through the experiment. The experiments were repeated several times with similar behaviour observed.

An important insight from this simple experiment is that the flow of gas through an unconsolidated, highly porous sand is a highly random process. The flow might be intermittent when one flow path is closed due to rearrangement of the sand grains or due to flow dynamics. The flow of air is also driven by a varying relative permeability for gas which depends on the liquid saturation in the sand. The lower the water-phase saturation is, the higher the permeability for gas could be, as demonstrated by Wyckoff and Botset (1936) for gas-liquid mixtures flowing through unconsolidated sand. This would agree with the observed accumulations of air and generation of new pathways in our experiment when a certain limit of gas saturation is reached. In general, the pathway through the sand (even for a thickness of less than half a meter) varies over time, and creates a high degree of randomness into the migration process. Similar unstable and fluctuating flow behaviour has also been observed in recent core-scale experiments reported by Reynolds and Krevor (2015) and Reynolds et al. (2018) who showed that CO_2-brine systems exhibit fluctuating flow paths at low, capillary-dominated flow rates. These fluctuating random flow paths of gases in granular pore systems are therefore widely observed and complex; being controlled by multiphase flow dynamics and heterogeneities in the granular pore systems. Characterising such flows in unconsolidated granular media is even more challenging than for consolidated rocks, since the medium itself can deform significantly.

4.5. Video observations at the seabed

During the underground blowout in 1989, video filming was used to monitor gas bubbles observed close to the well. Fig. 10 shows a still photo from the video clip taken at the seabed in December 1989. The video is taken close to the 2/4-13 well that is located 55 m Southeast of the 14-well. The 2/4-13 well was drilled to a depth of 2500 in 1988 and abandoned due to drilling problems. Several gas bubbles are observed on the photo (marked by a yellow arrow), and several small cavities are observed at the seabed. The diameter of these cavities is of the order of 2–3 cm. The cavity marked by a thick red arrow in Fig. 10 is the one where the gas bubbles originate from. Based on inspection from the video film, there are no visible bubbles escaping from the other cavities

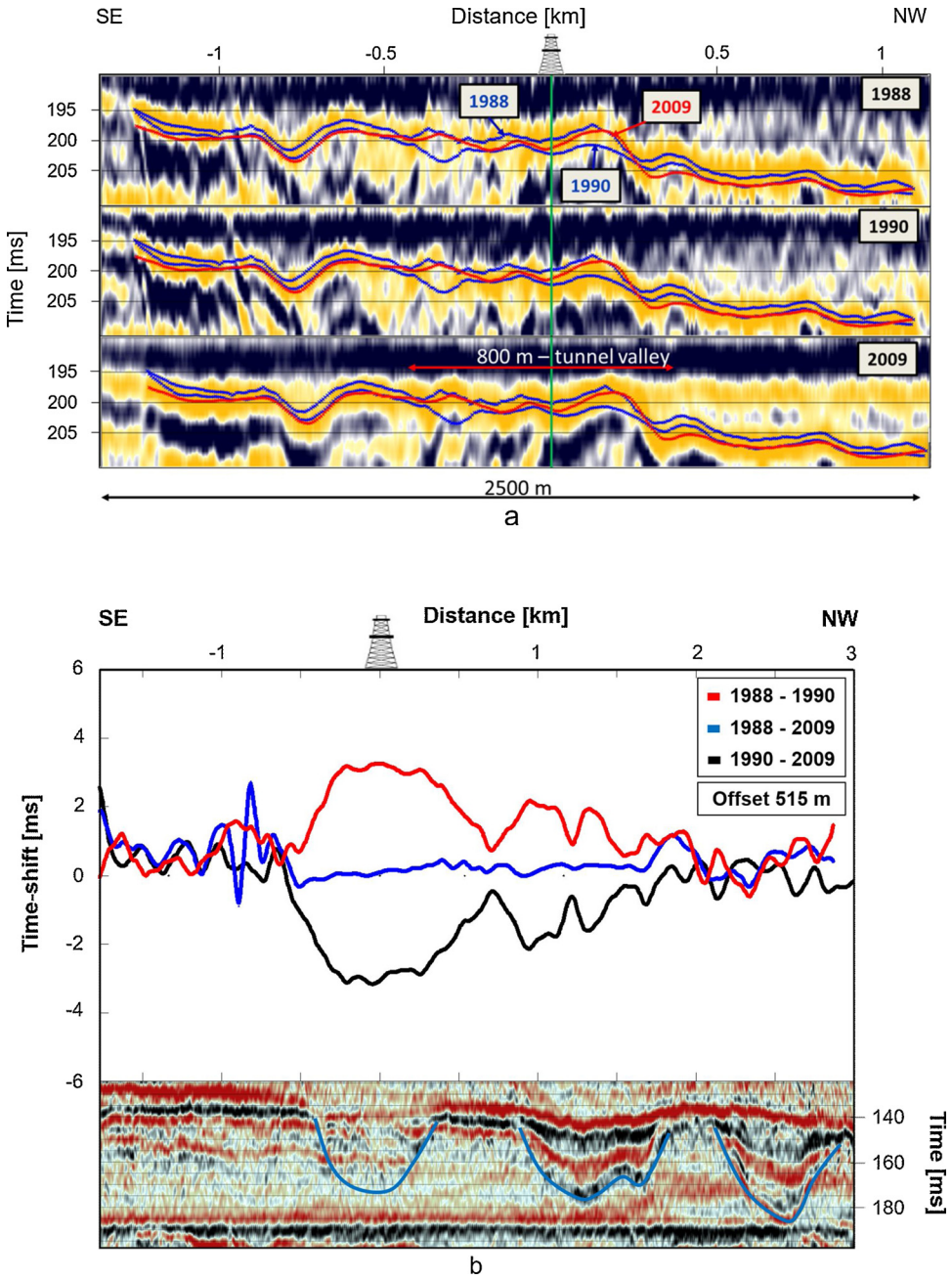

Fig. 8. a Automatic traveltime picks (maximum amplitude) for an interface below the shallow tunnel valleys (roughly 60 m below the tunnel valley and 95 m below seabed) for line B. Notice that the 2009 traveltimes (red solid line) are close to those in 1988 (prior to the blowout) for the area covered by the tunnel valley. For the area outside the tunnel valley, the traveltimes in 2009 are closer to the 1990 situation (1 year after the blowout). The vertical timescale for all three sections is from 190 to 210 ms. Fig. 8b Estimated time-lapse refraction timeshifts (using an offset of 515 m) using 3 repeated 2D lines from 1988 (pre blow out); 1990 (1 year after) and 2009 (20 years after) for line B. Notice a 3 ms time shift close to the well and tunnel valley (marked by a blue solid line in the lower seismic section) in 1990, and that this effect is close to zero when comparing 2009 and 1988 data.

(indicated by thinner red arrows on the figure). This might indicate that these cavities are not active any more, or that the bubbles escaping from these cavities are below optical resolution. At the wellhead of well 2/4-13 analysis of the gas bubbles showed that the gas was a mixture of biogenic (30–50%) and thermogenic (50–70%) gas.

This random pattern of cavities observed on video accords with our small-scale sand tank experiment in the sense that the process is random and that the cavities where the gas escapes into the water might vary as a function of time. The size of the cavity observed in the video photo is somewhat larger than in our sand tank experiment, 2–3 cm compared to 0.5 cm. It is hard to conclude whether these gas bubbles are caused by the 2/4-14 underground blow out or whether it represents natural seepage, or a combination of the two.

4.6. Passive seismic data compared with time lapse seismic

By integrating passive seismic data with the time-lapse seismic observations, we can further investigate the nature of an unstable shallow-gas migration event. In the period from 21st September to 3rd October 1989, four geophones were installed at the seabed close to the 2/4-14 well (Berteussen et al., 2006). Due to significant tilting of one of the geophones, only three were used for the analysis. Fig. 11 shows the location of the three geophones relative to wells 13 and 14. In Appendix A we show that it is possible to determine azimuth and apparent velocity from three geophone recordings, assuming that the observed seismic events are P-waves. We assume that the average P-wave velocity between the seabed and the sand layer at 490 m depth is approximately 1700 m/s (this is in estimated based on well logs in the area). The apparent velocity (Appendix A) is given as

$$v_a = \frac{v}{\cos\theta} \tag{1}$$

where θ is the inclination angle. If we assume that the source depth is known, we can use Eq. 1 and Eq. A7 (Appendix A) to estimate the position of a given event.

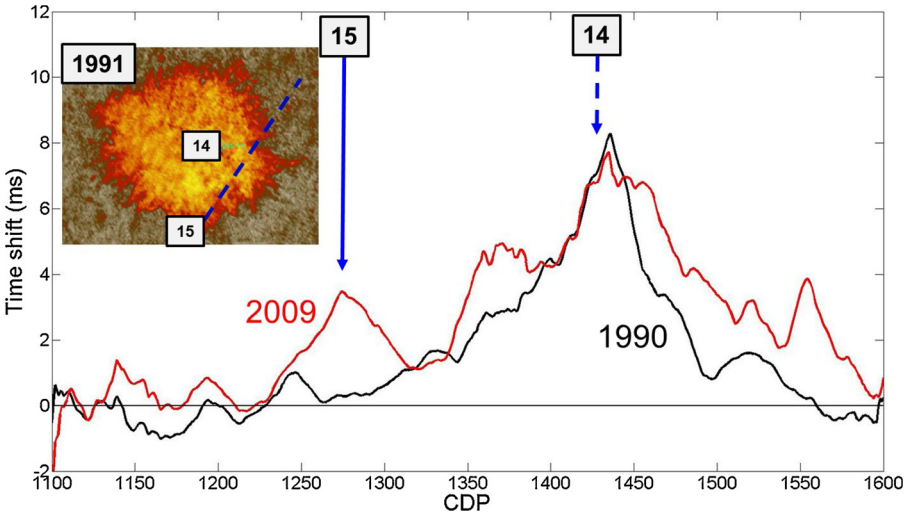

Fig. 9. Estimated seismic time shifts(relative to the 1988 data) for a reflector at approximately 600 m depth, clearly showing increased time shifts close to the 15-well between 1990 and 2009 for line C (dashed blue line in the inset). This is interpreted as vertical gas migration along the 15-well trajectory between 1990 and 2009. This figure is modified from Haavik and Landrø, 2014. The CMP-distance is 6.25 m, which means that the length of the line is 2.5 km.

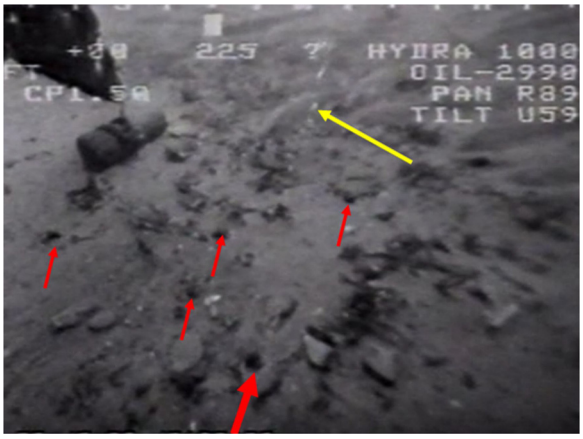

Fig. 10. Birds-eye view photo (snapshot from a video) showing gas bubbles (hardly visible; the yellow arrow point to one air bubble) escaping from the seabed close to the 2/4-14 well in December 1989. Red arrows indicate holes created by gas leakage. The thick red arrow indicates the root of the air bubbles (identified from the video clip). Close to the yellow arrow there are two small fish (also detecting the gas leakage!?).

Short periods of intense seismic activity (typically 30–60 min) were observed. More than 30 such periods were detected during these 13 days in 1989. This means that most of the time (more than 90%) there was silence, indicating a pulsating, episodic flow. The signal strength for these active periods could be up to 10 times the background noise level. By assuming that the seismic events occur at a depth of approximately 500 m, and that each event generates a seismic P-wave that propagates to the three geophones, it is possible to generate a location map, as shown in Fig. 12 (top). The maximum estimated range from the well to the furthest source position is approximately 600 m, corresponding to an inclination angle of 40 degrees, and an apparent velocity of approximately 2200 m/s. Based on the time-lapse seismic data observations, it is known that gas had entered into the thin sand layer at 490 m depth, and that the size of this gas anomaly was approximately 0.8 km in radius (see dashed blue line in Fig. 5). The acoustic events are spread within a radius of up to 600 m away from the well, and most events are observed to the southwest of the well. This map can be compared to time lapse seismic data (Fig. 12; bottom), where we observe some correlation between shallow time-lapse time shifts and the event location map. The time shifts were estimated for an interface at approximately 160 m (90 m below seabed) using data from 1988 and 1990 (October). From the time-lapse seismic analysis we interpret that gas has migrated into shallow sand layers, probably within the depth range from the seabed down to 90 m below. It is therefore likely that some gas had migrated into shallow gas layers by September 1989. However, it is very likely (based on the time shift analysis shown in Fig. 11; bottom) that there might have been shallower gas flow already occurring in September 1989. If this is the case the horizontal axis in Fig. 12 (top) should be modified towards lower *x*- and *y*-values.

A good correspondence between the two figures is observed in the sense that there are less events on the south-eastern side of the well, compared to the north-west. It should be noted that the 30-minute events described above appeared at very different locations, and that the map in Fig. 12 includes all events during the 13 days of passive seismic recording.

Berteussen et al. (2006) discuss an interesting observation for some of the seismic activity periods that were recorded in 1989. They state that the first tremors had an apparent velocity of approximately 2000 m/s lasting for approximately 5 min, followed by a relatively sudden (5–10 min) increase to apparent velocities around 5000–10000 m/s, with the bulk part of the seismic energy released within the next 40 min, then followed by a sudden decrease to apparent velocity back to 2000 m/s again, resulting in a U-shaped profile when apparent velocity is plotted against time, as shown in Fig. 12, and termed 'U-events'.

One possible way to obtain a qualitative understanding of these U-events, is to plot the apparent velocity versus inclination angle (Fig. 13). The apparent velocity increases significantly for inclination angles above 60 degrees. From this observation we suggest that the U-event shown in Fig. 12 can be interpreted as follows: the first 5–6 minutes are dominated by events that have a moderate inclination angle (around 40 degrees), followed by events that have inclination angles larger than 70 degrees for a period of approximately 40 min. At the final stage of the U-event the inclination angle is close to 40 degrees again. If we assume that the source depth causing the micro-seismicity is constant, these observations suggest distal acoustic sources at the beginning and end, and sources closer to the well for the middle period. This interpretation of the U-events is shown in Fig. 14. The sketch on the left shows (a) the initial phase where the gas front (after being stable for a certain amount of time) is pushed forward by the increased pressure caused by gas accumulation from the deep-sourced underground flow event. This phase lasts for approximately 5–6 min and is characterized by a relatively low apparent velocity (2000 m/s). In the next phase (b) the deeper or more central flow event becomes well established, and the dominant acoustic signal is from the part of the flow closer to the geophone array, probably from the vertical pathway. The amplitude level of the micro-seismic events are now 2–3 times stronger than those created in the initial phase (a). In the last phase (c) we suggest that the flow event starts dying out and that these last events

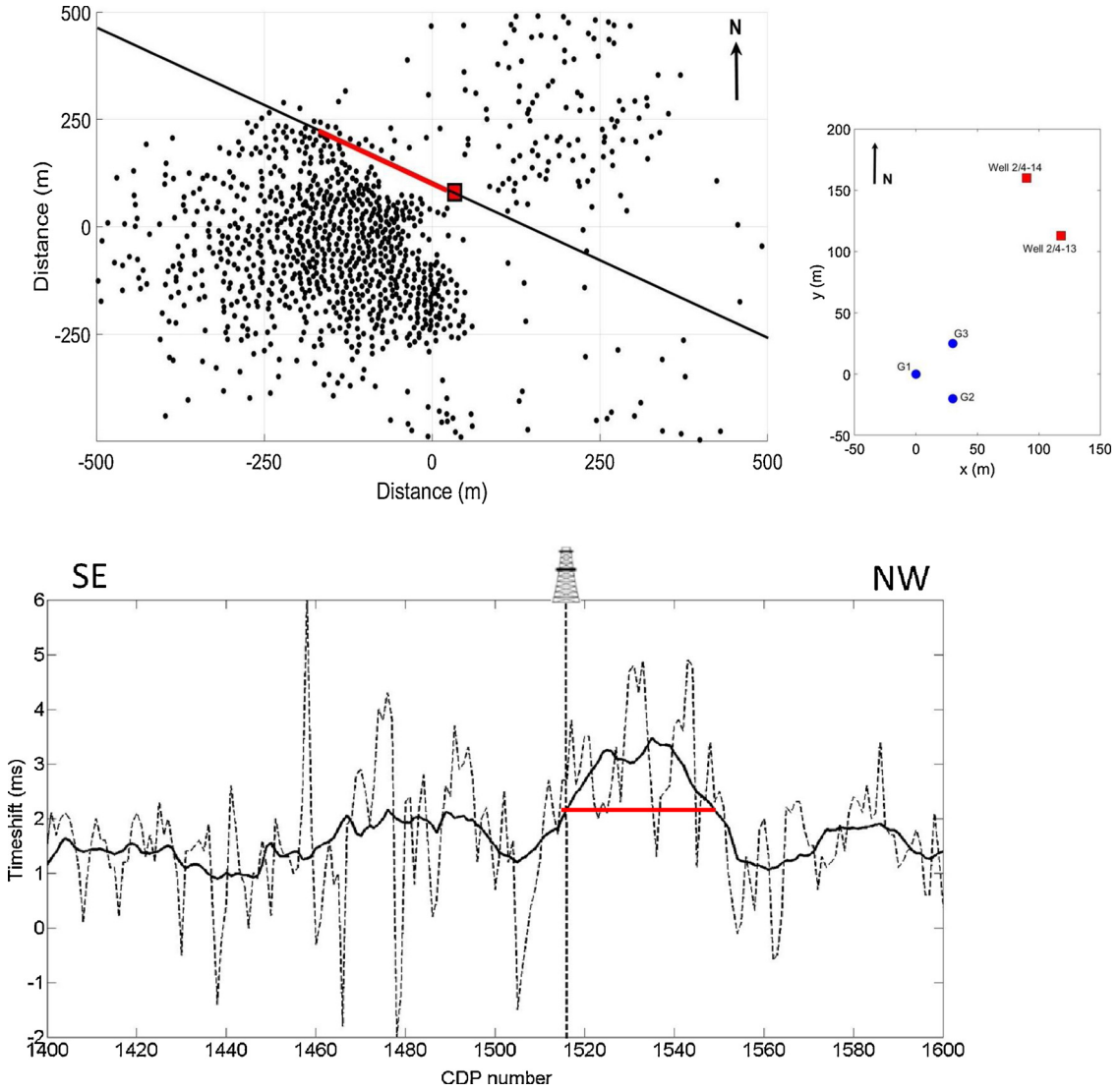

Fig. 11. Top left: seismic event map recorded in the period from 21st Septeber to 3rd October 1989 assuming that the depth of the seismic events is approximately 500 m. Notice that most events occur on the western side of the well (2/4-14 is marked in red). The seismic line is shown as the solid black line, and the area where larger time shifts are observed on the time lapse seismic data is shown by a thich red solid line. Top right: Location map of the three seabed geophones (blue circles) amd the 2/4-13 and 14 wells. Bottom: Estimated time shifts between 1988 and 1990 for the 2D line shown in black on the upper line. The CDP distance is 6.25 m, which means that the total length of the line shown in the bottom figure is 1250 m.

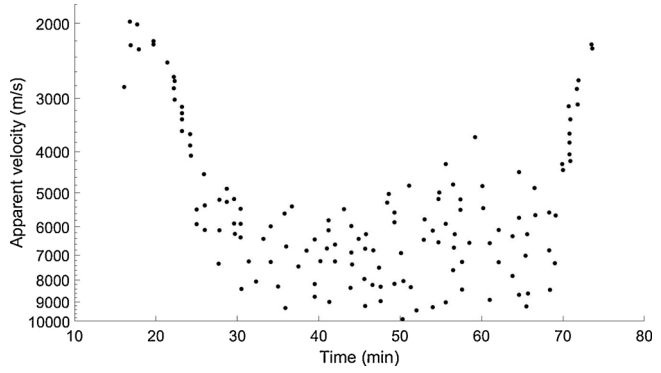

Fig. 12. Estimated apparent velocities versus trace number for an U-type event. For the first 5–6 min the apparent velocity is approximately 2000 m/s, then suddenly increasing to 7500 m/s and staying at this level for approximately 40 min, followed by a rapid change back to 2000 m/s again for the last 5 min.

occur close to the new gas front within the sand layer. Fig. 14 (right) shows a seismic amplitude map derived from the 3D seismic from 1991. This is used as an illustration to explain the interpretation of the first and last phase of the U-event: In the late phase the gas front spreads out, and according to the microseismic mapping, the azimuthal sector (as sketched by the two black lines in the figure) covers approximately 70 degrees from SW to W directions. Note that for this flow model, we assume that events occurred along both the vertical and the horizontal parts of the flow; however, the events close to the vertical chimney are dominant because they are closer to the geophone array. As the vertical flow decreases or stops, the signals created close to the 'delta-form' gas front become dominant.

4.7. Interpretation of gas flow events

Based on these time-lapse seismic observations, it is helpful to summarize the most likely interpretation of the sequence of shallow-gas migration events, as shown in Fig. 15. In April 1989 gas was flowing from the break in the casing at approximately 900 m depth, and migrating upwards along the outside of the well bore into the deep sand

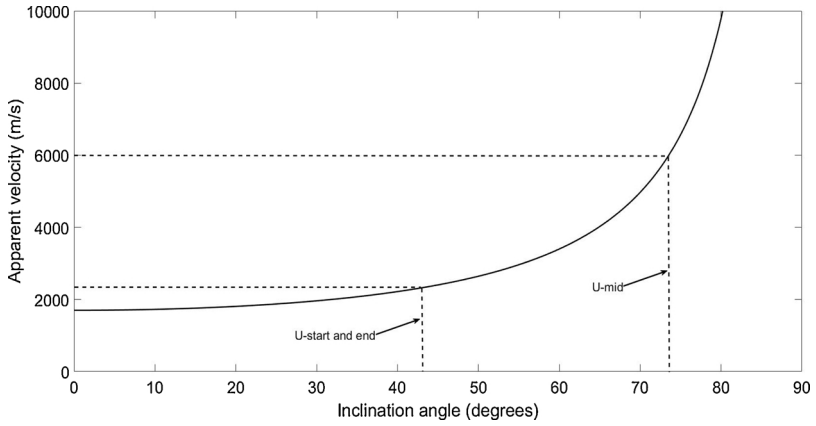

Fig. 13. Apparent velocity versus inclination angle. The dashed line shows that for the first and last phase of the U-event (Fig. 13) this angle is around 40–45 degrees, while the longer 40 min session inbetween has angles between 70 and 80 degrees.

layer at approximately 830 m depth. Due to the high permeability in this sand layer, the gas then migrated away from the well in a radial pattern, with probably more gas migrating in the up-dip direction (towards north east). Later, in October 1989 with continuing gas migration upwards along the well path, the gas then invaded and filled several shallower sand layers with gas. Again, in each high-porosity layer the gas migrated radially outwards, as sketched in Fig. 14. By October 1990, we assume that gas had migrated into the shallow tunnel valley and that some gas had also begun leaking directly into the water column. This last interpretation is based on the video clip observations showing gas bubbles close to the well in December 1989. Furthermore, based on seismic timeshift analysis we can assume that some gas had migrated into the tunnel valley and become trapped below a thin shale layer close to the top of the tunnel valley.

Table 1 summarizes various flow processes and lists the main geological recipients of the gas. The total amount of gas released from the blowout into shallow sediments is estimated to be between 200 and 370 MSm^3 (million standard cubic meters of gas). The numbers in Table 1 are given for in situ conditions, explicitely showing that gas at a depth of 830 m needs less space compared to atmospheric conditions. Since we lack 3D control of the tunnel valley geometry, it is hard to estimate the volume for this unit. However, we know that most of the gas went into the 830 m sand layer, hence the gas volume in the tunnel valley is most likely significantly less than 100 MSm^3.

The physical processes involved in these gas migration events are undoubtedly complex, but may be best understood in terms of migrating clusters of gas, termed ganglia. Stable accumulations of gas in water-wet porous media can be described by the balance of gravity and capillary forces, where an accumulation is stable if:

$$P_{th} > \delta\rho\, g\, h \quad (2)$$

where, P_{th} is the capillary threshold pressure of the sealing unit (e.g. silt or shale), $\delta\rho$ is the fluid density difference between gas and water and h is the accumulation height and g is the acceleration due to gravity.

The capillary threshold pressure is a function of the fluid interface and the pore throat radius (Washburn, 1921), such that:

$$P_{th} = 2\gamma \cos\theta / r \quad (3)$$

where γ is the interfacial tension between the fluid phases; θ is the contact angle between the gas phase and the rock and r is the pore throat radius for the rock unit (capillary seal). If the accumulation height increases such that the buoyancy force exceeds the capillary threshold pressure, then gas migration occurs, and a volume of gas migrates as a ganglion until a new stable accumulation is formed beneath a new capillary interface. The dynamics of migrating and accumulating gas ganglia in porous media are well described using invasion percolation concepts (Wilkinson and Willemsen, 1983) and have been successfully applied to analyses of the migration of various buoyant non-wetting fluids (e.g. oil, gas or CO_2) in water-filled porous media (Frette et al., 1992; Carruthers and Ringrose (1998); Cavanagh and Ringrose, 2011; Cavanagh and Haszeldine, 2014). A key aspect of the process is 'snap-off' within an initially continuous gas cluster creating separate gas clusters (which may later merge to form new accumulations). The migrating gas phase is therefore generally non-continuous and cannot be described using continuum flow theory.

In conventional invasion percolation studies, it is assumed that the porous medium has constant properties and that the flow dynamics are controlled by the supply rate of the non-wetting buoyant fluid phase. However, in the case of shallow gas migration in unconsolidated

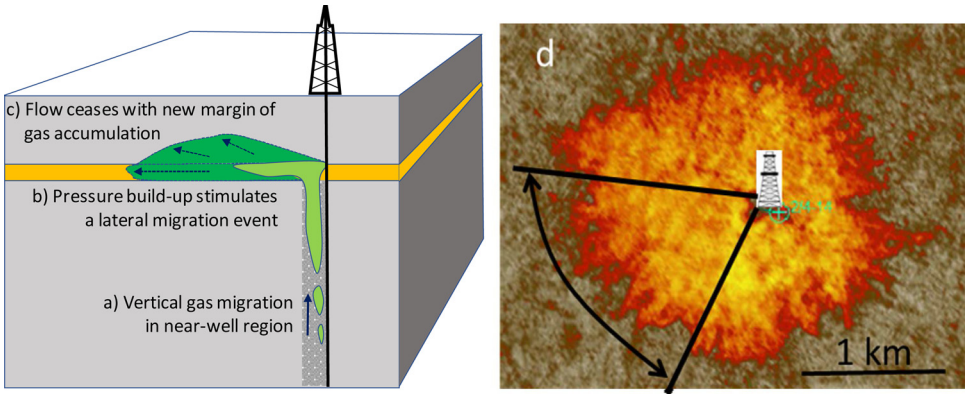

Fig. 14. Interpretation of the U-type passive-seismic event (left-hand figure): a) A gradual build-up of pressure in the initial accumulation caused by gas migration in the near-well region triggers a migration pulse at the upper water-gas contact (lasting for 5–6 minutes); b) the migration pulse from the vertical feeder continues for 35 min; (c) in the last 5 min the flow pulse terminates, first close to well, and ending with a new gas-water interface further away from the well. The azimuthal distribution of the U-type event is shown in the right-hand figure, where the sector for the passive seismic events is shown, overlain on the seismic amplitude map of the gas-charged sand layer at 492 m. This azimuthal variation might explain why some late microseismic events occur close to the edge of the gas filled region. The amplitude map is based on 3D seismic data from 1991, so the areal extent of this layer was probably less in September/October 1989.

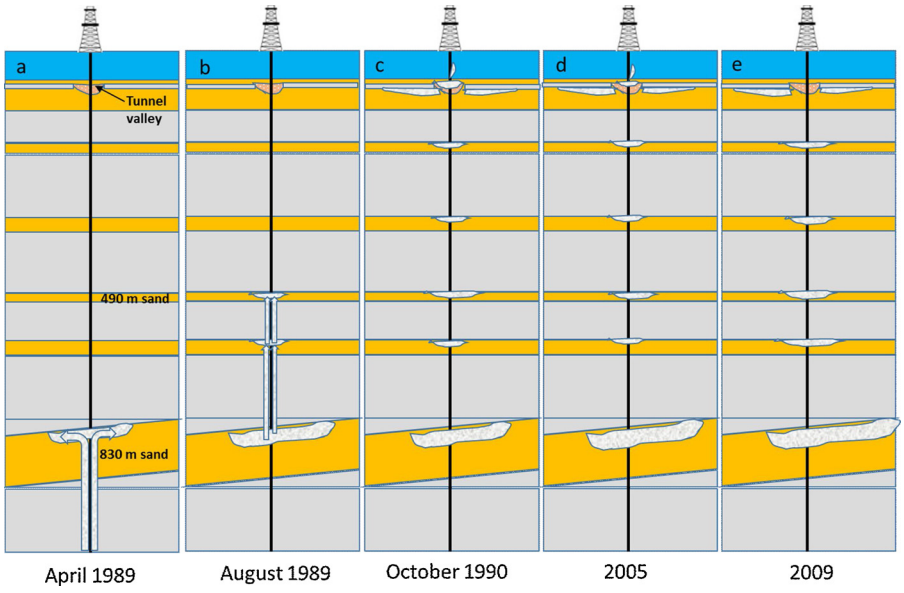

Fig. 15. Interpretation of gas migration versus calendar time based on time lapse seismic data and the video clip from the seabed close to the well in December 1989. Note that the actual number of sand/silt-layers are higher than indicated here, and also the relative positions between layers are far from exact. Note that the deep sandlayer is upward dipping towards NorthEast.

sediments, as described here, this may not be the case. In unconsolidated sediments, the increase in gas pressure at the crest of an accumulation may cause deformation of the granular medium (increasing pore throat apertures), resulting in a capillary interface with a threshold pressure, P_{th}, which can vary as a function of time. We therefore infer that the U-type event described here involves a migrating pulse of gas migrating within a granular medium that it also deformed by the migrating gas (causing acoustic events). The dynamics of such a complex process is not fully understood, but the seismic observations clearly indicate the detection of a gas migration event.

Using Eq. 2 and fluid density estimates from Fig. 1, we can estimate the confining pressure (P_{th}) for the shallow U-type event to be around 21 bars (2.1 MPa), immediately prior to the migration event. Using Eq. 3, along with empirical relationships between P_{th} and permeability (published by Manzocchi et al., 2002) we can estimate that the sealing layer must have had a permeability of around 0.1 microdarcy (10^{-20} m^2) – a reasonable value for a shale layer at this depth of burial. The seismic U-event was probably related to the breaching of that seal and re-migration to a new quasi-stable gas accumulation.

5. Discussion

In the area close to the 2/4-14 well there are numerous gas accumulations (Haavik and Landrø, 2014). One trapping mechanism for such gas pockets is created by intersecting iceberg plough marks digging into slightly dipping sand layers. Dowdeswell and Ottesen (2013) show that buried iceberg plough marks can contain accumulations of natural gas. It is therefore not certain that the gas observed close to the well originates from the 2/4-14 underground blowout, since there is a certain probability that this is sourced from natural seepage. The gas bubbles observed close to the 2/4-13 well in December 1989 was a mixture of biogenic and thermogenic gas. Hence we cannot conclude that these bubbles originate only from the 14-well. However, when this information is linked to the time-lapse seismic observations, it is likely that some gas originates from the 14 well. The short distance to the 14-well (55 m) strengthens this assumption.

The interpretation sketch shown in Fig. 15 (not exactly to scale) is designed to summarize our most likely interpretations, based on time-lapse seismic data, passive seismic data and the seabed observations. We have proposed a process of migrating gas ganglia in a deformable porous medium as the most likely model, but further work on flow modeling and interpretation of the observed gas-flow dynamics is clearly needed.

Based on site survey data for time-lapse seismic analysis, the repeatability level in this study is reduced compared to conventional 4D seismic data (in deeper consolidated rocks). The repeatability is also reduced when the position of the source and receivers changes between the base and monitor surveys, as shown by Landrø, 1999. However, in our case, the effect of gas entering into a sand layer gives a strong 4D effect so that the relatively poor repeatability is compensated by the strong fluid effects. Furthermore, we think that time shift analysis is less influenced by inaccurate positioning than amplitude differences, especially since the shallow subsurface is mostly (apart from tunnel valleys and ice scours) composed of near to horizontal sedimentary layers.

The relief well scenario described in this paper is relevant to carbon storage in several ways. First, if the pore pressure at an injection site is increased due to low injectivity, it might be necessary to drill a pressure "relief" well to produce water (below the CO_2-water contact within the storage volume) to lower the pressure. It is extremely unlikely that the pore pressure within a CO_2-storage site will reach as high pressures as

Table 1
Overview of gas migration and flow processes involved in the 2/4-14 underground blowout incident. Volume estimates are based on spinner measurements and estimated areal extent of gas anomalies from seismic data. There are significant uncertainties related to the volume estimates.

Depth of observation	Approximate gas volume (in situ) end 1989	Approximate gas volume (in situ) 2009	Flow process observed
830 m sand	3.3 Mm^3	3.1 Mm^3	Lateral migration from wellbore leakage event
490 m sand	0.6 Mm^3	0.9 Mm^3	Lateral migration from wellbore leakage event
100 m tunnel valley	No 3D control, some gas in 1990	Less (close to zero) than in 1990	Lateral migration from wellbore leakage event and subsequence re-migration
Near-wellbore damage zone	300 m^3 (assuming 1 m radius)	100 m^3 (estimate based on seismic timeshifts)	Continued migration feeding shallow layers and surface migration
Seabed	0.1-15 m^3 (assuming 1 mm and 5 mm bubble radius)	Less than 1989 and close to zero	Episodic flows

in our blow out example (1050 bars). The relief well scenario is also relevant in cases where it is planned to store CO_2 in abandoned hydrocarbon reservoirs. In such cases there might be several leagcy wells penetrating the reservoir unit, increasing the risk of vertical migration outside the well bore, as described in this paper. More generally, improved understanding of shallow gas migration processes is important for designing CO_2 storage projects and their monitoring programmes.

Based on the observations from this paper and the simulation work presented by Langseth and Landrø (2012) we find that the current study *indicates* that the gas flow in the shallow sediments approached a static situation after 20 years. One way to strengthen this hypothesis is to acquire new seismic data sets in the area, to determine if there are any changes from 2009 to date.

6. Conclusions

We have shown that time-lapse seismic data serve as an efficient tool to monitor subsurface gas flow in shallow sediment sequences, and can provide an effective tool for interpreting gas flow over several years following this underground blow-out event. Furthermore, this monitoring approach is strengthened by using passive seismic data that were recorded approximately 8 months after the uncontrolled flow started. We find that most of the gas that leaked from the deep reservoir becomes trapped in shallow sand layers within the first kilometre below the seabed. The actual gas-flow pattern that can be interpreted from the geophysical data is a combination of vertical propagation close to wells and lateral migration of gas within several thin sand layers. These examples illustrate the complexity of shallow gas migration and leakage events, and provide a better basis for efforts to understand gas and CO_2 migration processes in shallow sediment sequences. Key processes observed are the retention of migrated gas in multiple high-porosity layers and structural traps, vertical migration along disturbed zones around wells, and the episodic nature of gas migration in heterogeneous sedimentary sequences. Thin shales acting as containment barriers to these gas accumulations probably had permeabilities of the order of 0.1 microdacry, and were periodically breached or ruptured in gas migration events. These migration processes have been successfully modelled by others using invasion percolation models of migrating buoyant gas ganglia; however, the concurrent deformation of the medium in unconsolidated sedimentary sequences presents a new challenge for modelling the flow dynamics.

Acknowledgments

Kristian Kolbjørnsen is acknowledged for numerous positive discussions. Sadly, he passed away in February 2019. We want to thank AkerBP, CGG, Lundin Norway, Equinor (formerly Statoil) and Total for financial support and making data available to the LOSEM project at NTNU. Daniel Wehner acknowledges support from EU Horizon 2020 research and innovation programme under the grant agreement, No 641943 through the WAVES consortium. This work was partly funded by the Norwegian Research Council, through the CLIMIT program, under grant no. 254748 “Distributed seismic monitoring for geological carbon sequestration”, and the industry partners Equinor and Octio. Massoud Ibraheem is acknowledged for improving Figs. 11 and 12 based on old paper copy plots. The reviewers, Jonathan Bull and one anonymous are acknowledged for constructive and helpful suggestions that improved the paper significantly.

Appendix A. Estimating azimuth and apparent velocity from 3 geophones

If we assume that the acoustic sources caused by the underground flow acts as point sources at a given source location $R_s = (x_s, y_s, z_s)$ and that the position of the three geophones are given as $g_i = (x_i, y_i, 0)$, assuming that the seabed level corresponds to $z = 0$. If we restrict our analysis to P-waves only, and assume a constant P-wave velocity v, then we find that the travel times from an arbitrary source location to each of the three receivers are given as:

$$T_i = \frac{1}{v}\sqrt{(x_s - x_i)^2 + (y_s - y_i)^2 + z_s^2};\ i = 1, 2, 3. \tag{A1}$$

Since we do not know when the source is activated, we can only measure two independent travel-time shifts from the three geophone recordings, for instance $\Delta T_{12} = T_2 - T_1$ and $\Delta T_{13} = T_3 - T_1$. The third possible traveltime shift, $\Delta T_{23} = T_3 - T_2 = \Delta T_{13} - \Delta T_{12}$ is a combination of the two others and hence not an independent measurement. This means that we can determine two independent traveltime differences from the three geophone recordings.

Now, we consider an incoming P-wave propagating from a source depth z_s that has an inclination angle θ to the seabed surface (Fig. A1). Assuming a flat seabed at $z = 0$, we define the apparent velocity of an incoming P-wave that makes an angle θ (inclination angle) to this surface as the distance between the two rays (Δx) in the z = 0 plane divided by the traveltime difference:

$$v_a = \frac{\Delta x}{\Delta t} \tag{A2}$$

The traveltime difference in the denominator is given as (assuming that $\Delta x \ll r_1; r_2$)

$$\Delta t = (r_2 - r_1)/v \approx \frac{x\Delta x}{v\sqrt{x^2 + z_s^2}} \tag{A3}$$

Inserting Eq. A3 into A2 we find that the apparent velocity is given as

$$v_a = \frac{v}{\cos\theta} \tag{A4}$$

In the seabed plane we introduce the apparent slowness $u = \frac{1}{v_a}$, which is a vector in the z = 0 plane. The two traveltime differences are now given as

$$\Delta T_{12} = u_x(x_2 - x_1) + u_y(y_2 - y_1) \tag{A5}$$

$$\Delta T_{13} = u_x(x_3 - x_1) + u_y(y_3 - y_1) \tag{A6}$$

In Eqs. A5 and A6 we assume the traveltime differences are measured and the geophone positions are known. This means that we can estimate the two slowness vector components directly from these two equations. This gives a unique determination of the azimuth angle ϕ and the apparent velocity:

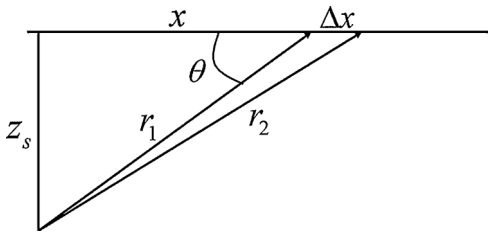

Fig. A1. Two incoming P-waves recorded at receiver locations separated by a distance Δx. The angle to the seabed plane, θ, is the inclination angle.

$$\tan\phi = \frac{u_x}{u_y} \tag{A7}$$

$$v_a = \frac{1}{\sqrt{u_x^2 + u_y^2}} \tag{A8}$$

This means that the geophone array can determine the azimuth and the apparent velocity of each event, and that it is not possible to determine the depth and the *x*-*y*-position simultaneously. However, we can assume that the depth is known, and in our case example we know from seismic data analysis that the gas front in September 1989 was close to circular shaped at a depth of 490 m. This assumption has been used to produce Fig. 12. However, it is very likely (based on 4D refraction analysis) that some gas has migrated into sand layers shallower than 490 m.

.

References

Arntsen, B., Wensaas, L., Løseth, H., Hermanrud, C., 2007. Seismic modeling of gas chimneys. Geophysics 72, SM251–SM259.

Benson, S., Hepple, R., 2005. Detection and options for remediation of leakage from underground CO_2 storage projects. Greenhouse Gas Control Technol. 7, 1329–1335.

Berteussen, K.A., Kolbjørnsen, K., Larsen, D.A., Kristiansen, P., 2006. Monitoring of an Uncontrolled Gas Flow by Sea Bottom Seismic Instruments – A North Sea Case Study. Extended Abstract A16, EAGE Workshop on Passive Seismic, Dubai December 2006.

Blackford, J., Stahl, H., Bull, J.M., Berges, B.J.P., Cevatoglu, M., Lichtschlag, A., Connelly, D., James, R.H., Kita, J., Long, D., Naylor, M., Shitashima, K., Smith, D., Taylor, P., Wright, I., Akhurst, M., Chen, B., Gernon, T.M., Hauton, C., Hayashi, M., Kaieda, H., Leighton, T.G., Sato, T., Sayer, M.D.J., Suzumura, M., Tait, K., Vardy, M.E., White, P.R., Widdicombe, S., 2014. Detection and impacts of leakage from sub-seafloor deep geological carbon dioxide storage. Nat. Clim. Change 4, 1011–1016.

Calvert, R., 2005. Insights and methods for 4D reservoir monitoring and characterization. EAGE/SEG Distinguished Instructure Short Course. pp. 8.

Carruthers, D., Ringrose, P., 1998. Secondary oil migration: oil-rock contact volumes, flow behaviour and rates. Geol. Soc. Lond. Spec. Publ. 144 (1), 205–220.

Cavanagh, A.J., Haszeldine, R.S., 2014. The Sleipner storage site: capillary flow modeling of a layered CO_2 plume requires fractured shale barriers within the Utsira Formation. Int. J. Greenhouse Gas Control. 21, 101–112.

Cavanagh, A., Ringrose, P., 2011. Simulation of CO2 distribution at the in Salah storage site using high-resolution field-scale models. Energy Procedia 4, 3730–3737.

Cevatoglu, M., Bull, J.M., Vardy, M.E., Gernon, T.M., Wright, I.C., Long, D., 2015. Gas migration pathways, controlling mechanisms and changes in sediment acoustic properties observed in a controlled sub-seabed CO2 release experiment. Int. J. Greenhouse Gas Control. 38, 26–43.

Dowdeswell, J.A., Ottesen, D., 2013. Buried iceberg ploughmarks in the early Quaternary sediments of the central North Sea: a two-million year record of glacial influence from 3D seismic data. Mar. Geol. 344, 1–9.

Etiope, 2015. Natural Gas Seepage – The Earth's Hydrocarbon Degassing. Springerhttps://doi.org/10.1007/978-3-319-14601-0_1.

Frette, V., Feder, J., Jøssang, T., Meakin, P., 1992. Buoyancy-driven fluid migration in porous media. Phys. Rev. Lett. 68 (21), 3164.

Furre, A.K., Ringrose, P., Cavanagh, A., Janbu, A.D., Hagen, S., 2014. Characterisation of a submarine glacial channel and related linear features. Near Surface Geoscience 2014-First Applied Shallow Marine Geophysics Conference.

Grimstad, A.A., Georgescu, S., Lindeberg, E., Vuillaume, J.F., 2009. Modelling and simulation of mechanisms for leakage of CO2 from geological storage. Energy Procedia 1 (1), 2511–2518.

Haavik, K.E., Landrø, M., 2014. Iceberg ploughmarks illuminated by shallow gas in the central North Sea. Quat. Sci. Rev. 103, 34–50.

Hovland, M., Judd, A.G., 1988. Seabed Pockmarks and Seepages. Impact on Geology, Biology and the Marine Environment. Graham and Trotman Ltd. London 293 pp.

Landrø, 1999. Repeatability issues of 3-D VSP data. Geophysics 64, 1673–1679.

Landrø, M., Solheim, O.A., Hilde, E., Ekren, B.O., Strønen, L.K., 1999. The gullfaks 4D study. Pet. Geosci. 5, 213–226.

Landrø, M., 2011. Seismic monitoring of an old underground blowout – 20 years later. First Break. 29, 39–48.

Landrø, M., 2015. 4D seismic, chapter 19. In: Bjørlykke, K. (Ed.), Petroleum Geoscience, second edition. Springer, pp. 489–514 ISBN 978-3-642-34131-1.

Landrø, M., Zumberge, M., 2017. Estimating saturation and density changes caused by CO2 injection at Sleipner – using time-lapse seismic amplitude-variation-with-offset and time-lapse gravity. Interpretation 5, T243–T257.

Langseth, E., Landrø, M., 2012. Time-lapse 2D interpretation of gas migration in shallow sand layers – compared to reservoir simulation. Int. J. Greenhouse Gas Control 10, 389–396.

Larsen, D.O., Lie, A., 1990. Monitoring an underground flow by shallow seismic data: a case study. 60th SEG Annual Mtg., Expanded Abstracts. pp. 201–202.

Manzocchi, T., Heath, A.E., Walsh, J.J., Childs, C., 2002. The representation of two phase fault-rock properties in flow simulation models. Pet. Geosci. 8 (2), 119–132.

Moser, T.J., Arntsen, B., Johansen, S., Raknes, E.B., Sangesland, S., 2016. Surface seismic monitoring while drilling using diffractions – concept and field data example. Seg Tech. Program Expand. Abstr. 2016, 662–666.

Naylor, M., Wilkinson, M., Haszeldine, R.S., 2011. Calculation of CO_2 column heights in depleted gas fields from known pre-production gas column heights. Mar. Pet. Geol. 28 (5), 1083–1093.

Nooner, S.L., Eiken, O., Hermanrud, C., Sasagawa, G.S., Stenvold, T., Zumberge, M.A., 2007. Constraints on the in situ density of CO 2 within the Utsira formation from time-lapse seafloor gravity measurements. Int. J. Greenhouse Gas Control. 1 (2), 198–214.

Reynolds, C.A., Krevor, S., 2015. Characterizing flow behavior for gas injection: relative permeability of CO2-brine and N2-water in heterogeneous rocks. Water Resour. Res. 51 (12), 9464–9489.

Reynolds, C.A., Blunt, M.J., Krevor, S., 2018. Multiphase Flow Characteristics of Heterogeneous Rocks From CO2 Storage Reservoirs in the United Kingdom. Water Resour. Res. 54, 729–745.

Salem, H.S., 2000. Poisson's ratio and the porosity of surface soils and shallow sediments, determined from seismic compressional and shear wave velocities. Geotechnique 50 (4), 461–464.

Singh, V.P., Cavanagh, A., Hansen, H., Nazarian, B., Iding, M., Ringrose, P.S., 2010. Reservoir modeling of CO2 plume behavior calibrated against monitoring data from Sleipner, Norway. January. SPE Annual Technical Conference and Exhibition. Society of Petroleum Engineers.

Stewart, M.A., Lonergan, L., Hampson, G., 2013. 3D seismic analysis of buried tunnel valleys in the Central North Sea: morphology, cross-cutting generations and glacial history. Quat. Sci. Rev. 72, 1–17.

van der Vegt, P., Janszen, A., Moscariello, A., 2012. Tunnel valleys: current knowledge and future perspectives. In: In: Huuse, M., Redfern, J., Le Heron, D.P., Dixon, R.J., Moscariello, A., Craig, J. (Eds.), Glaciogenic Reservoirs and Hydrocarbon Systems. Geological Society, vol. 368. Special Publications, London, pp. 75–97.

Washburn, E.W., 1921. The dynamics of capillary flow. Phys. Rev. 17, 273–283.

Wilkinson, D., Willemsen, J.F., 1983. Invasion percolation: a new form of percolation theory. J. Phys. A Math. Gen. 16 (14), 3365.

Wyckoff, R.D., Botset, H.G., 1936. The flow of gas-liquid mixtures through unconsolidated sands. J. Appl. Phys. 7 (9), 325–345.

Zadeh, H.M., Landrø, M., 2011. Monitoring a shallow subsurface gas flow by time-lapse refraction analysis. Geophysics 76, O35–O43.